Supplementary data

A brain atlas of axonal and synaptic delays based on modelling of cortico-cortical evoked potentials

Jean-Didier Lemaréchal et al. - F-TRACT consortium

Correspondence

Olivier David, PhD
Institut de Neurosciences des Systèmes - Faculté de Médecine - 27, boulevard Jean Moulin - 13005 Marseille, France
Email: Olivier.David@inserm.fr

Supplementary data are divided into 2 sections. The first section details the neural mass model used to estimate the CCEPs parameters, along with the equations of its dynamics. The second section provides supplementary figures.

I The ERP neural mass model

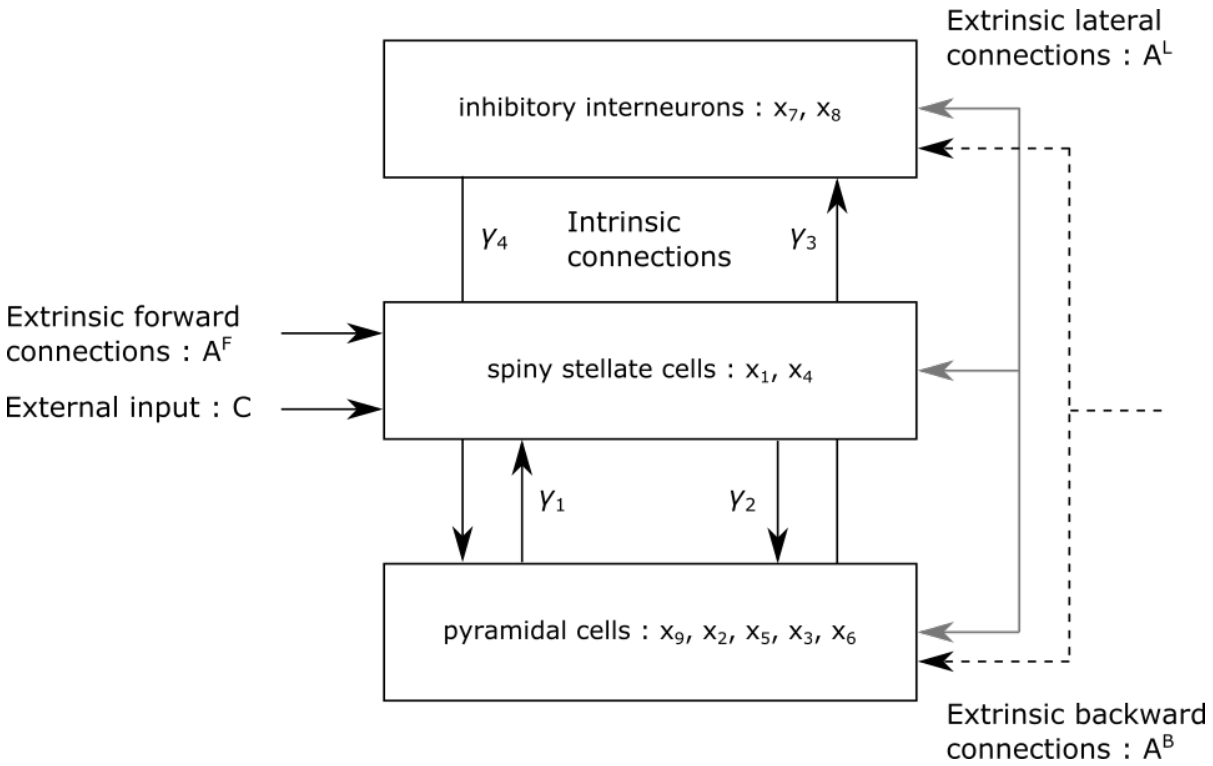

Supplementary Fig. 1 Single region model. Each region is modeled with three neuronal populations (pyramidal cells, spiny stellate cells and inhibitory interneurons). The dynamics of each population is described by a set of state variables {x}. Populations are coupled with intrinsic connections γ_k. The region also receives an external input and different types of extrinsic connections (forward, backward, lateral), originating from other regions and targeting specific populations.[1] This figure is associated to section Materials and methods (Estimation of axonal conduction delays and synaptic time constants).

The following presents the system of delay differential equations used to characterize the dynamics of a brain area *i* in the ERP neuronal model.[1,2] The dynamics of the region (Supplementary Fig. 1) is described by the temporal evolution of a global state vector $x = \{x_1, x_2, x_3, x_4, x_5, x_6, x_7, x_8, x_9\}$. The specific parameters were are focusing on are $\left\{\tau_e^{(i)}, \tau_i^{(i)}\right\}$, the excitatory and inhibitory synaptic time constants of area *i* and $\left\{\delta^{(ij)}\right\}$, the axonal conduction delay from area *j* to area *i*.

Inhibitory interneurons :

$\dot{x}_7^{(i)}(t) = x_8^{(i)}(t)$

$$\dot{x}_8^{(i)}(t) = \frac{H_e^{(i)}}{\tau_e^{(i)}}\left[\sum_{\substack{j=1 \\ j\neq i}}^{n_s} A^B(i,j)S\left(x_9^{(j)}\left(t-\delta^{(ij)}\right)\right) + \sum_{\substack{j=1 \\ j\neq i}}^{n_s} A^L(i,j)S\left(x_9^{(j)}\left(t-\delta^{(ij)}\right)\right) + \gamma_3 S\left(x_9^{(i)}\left(t-\delta^{(ii)}\right)\right)\right] - \frac{2}{\tau_e^{(i)}}x_8^{(i)}(t) - \frac{x_7^{(i)}(t)}{\tau_e^{(i)2}}$$

Spiny stellate cells:

$$\dot{x}_1^{(i)}(t) = x_4^{(i)}(t)$$

$$\dot{x}_4^{(i)}(t) = \frac{H_e^{(i)}}{\tau_e^{(i)}}\left[\sum_{\substack{j=1 \\ j\neq i}}^{n_s} A^F(i,j)S\left(x_9^{(j)}\left(t-\delta^{(ij)}\right)\right) + \sum_{\substack{j=1 \\ j\neq i}}^{n_s} A^L(i,j)S\left(x_9^{(j)}\left(t-\delta^{(ij)}\right)\right) + C(i)u^{(i)}(t) + \gamma_1 S\left(x_9^{(i)}\left(t-\delta^{(ii)}\right)\right)\right] - \frac{2}{\tau_e^{(i)}}x_4^{(i)}(t) - \frac{x_1^{(i)}(t)}{\tau_e^{(i)2}}$$

Pyramidal cells:

$$\dot{x}_9^{(i)}(t) = x_5^{(i)}(t) - x_6^{(i)}(t)$$

$$\dot{x}_2^{(i)}(t) = x_5^{(i)}(t)$$

$$\dot{x}_5^{(i)}(t) = \frac{H_e^{(i)}}{\tau_e^{(i)}}\left[\sum_{\substack{j=1 \\ j\neq i}}^{n_s} A^B(i,j)S\left(x_9^{(j)}\left(t-\delta^{(ij)}\right)\right) + \sum_{\substack{j=1 \\ j\neq i}}^{n_s} A^L(i,j)S\left(x_9^{(j)}\left(t-\delta^{(ij)}\right)\right) + \gamma_2 S\left(x_1^{(i)}\left(t-\delta^{(ii)}\right)\right)\right] - \frac{2}{\tau_e^{(i)}}x_5^{(i)}(t) - \frac{x_2^{(i)}(t)}{\tau_e^{(i)2}}$$

$$\dot{x}_3^{(i)}(t) = x_6^{(i)}(t)$$

$$\dot{x}_6^{(i)}(t) = \frac{H_i^{(i)}}{\tau_i^{(i)}}\gamma_4 S\left(x_7^{(i)}\left(t-\delta^{(ii)}\right)\right) - \frac{2}{\tau_i^{(i)}}x_6^{(i)}(t) - \frac{x_3^{(i)}(t)}{\tau_i^{(i)2}}$$

With:

$x_k^{(i)}(t)$: k^{th} state of the system for brain area i at instant t. Nine state variables are typically used in DCM for ERP.

$u^{(i)}(t)$: burst of extrinsic input entering the system

$S(x)$: nonlinear transformation of postsynaptic potential into firing rate

A^F, A^B, A^L, C: extrinsic forward, backward, lateral and input coupling

$H_e^{(i)}, H_i^{(i)}$: excitatory and inhibitory synaptic receptor density

$\gamma_1, \gamma_2, \gamma_3, \gamma_4$: intrinsic coupling

The specific time-related parameters are:

$\tau_e^{(i)}, \tau_i^{(i)}$: excitatory and inhibitory synaptic time constants

$\delta^{(ii)}$: intrinsic conduction delay (between neuronal populations of area *i*)

$\delta^{(ij)}$: extrinsic conduction delay (from area *j* to area *i*)

II Supplementary figures

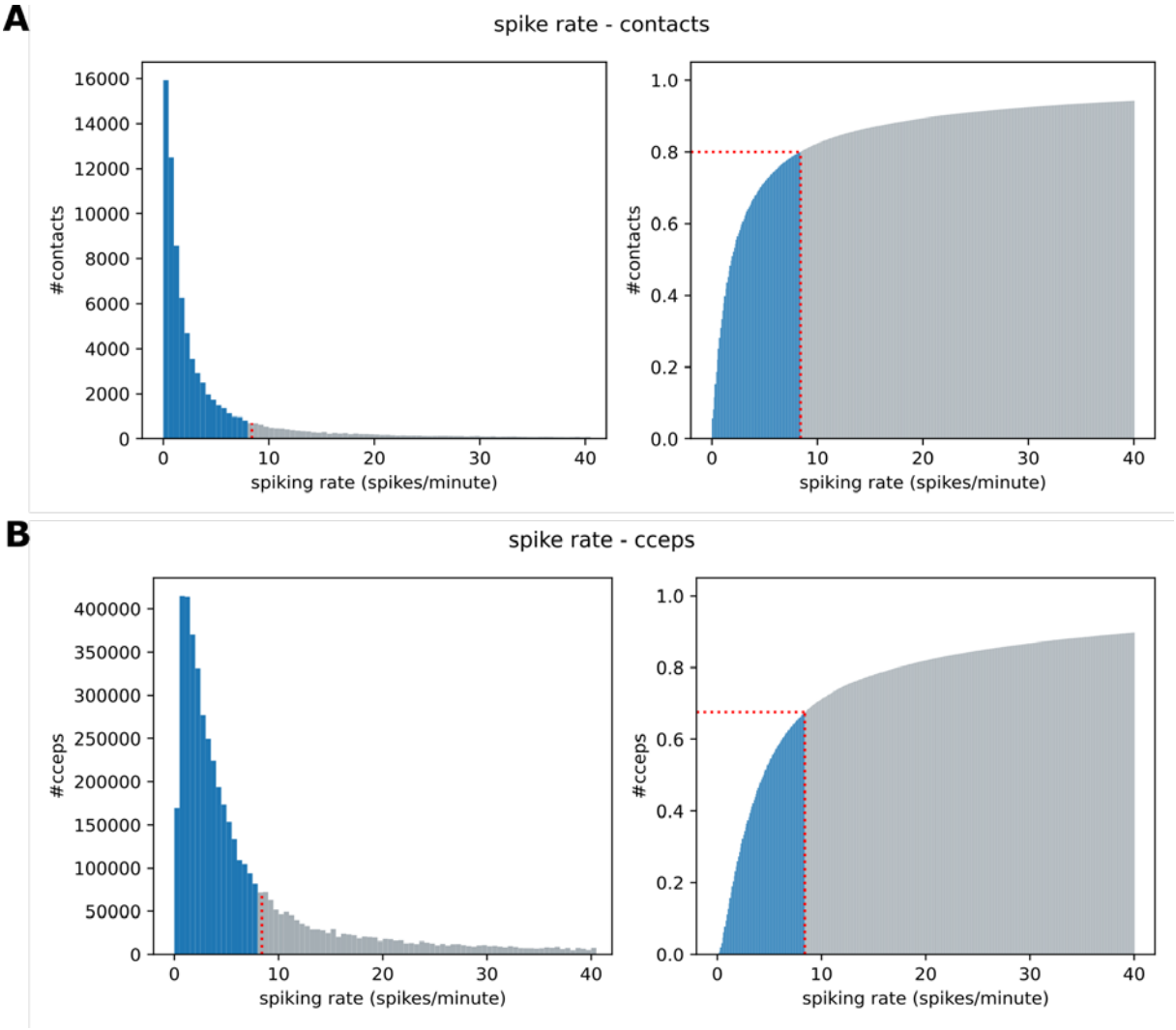

Supplementary Fig. 2 Estimation of contact spiking rate. The spiking rate of each contact is estimated from interictal recordings, using Delphos (Detector of ELectroPHysiological Oscillations and Spikes).[3] A maximum spiking rate threshold of 8.4 spikes per minute, indicated by the red dotted line in the histogram (A, left) and the cumulative distribution (A, right) allows to save 80% of contacts (blue regions). The rejection of 20% of contacts results in the rejection of 33% of CCEPs (B).

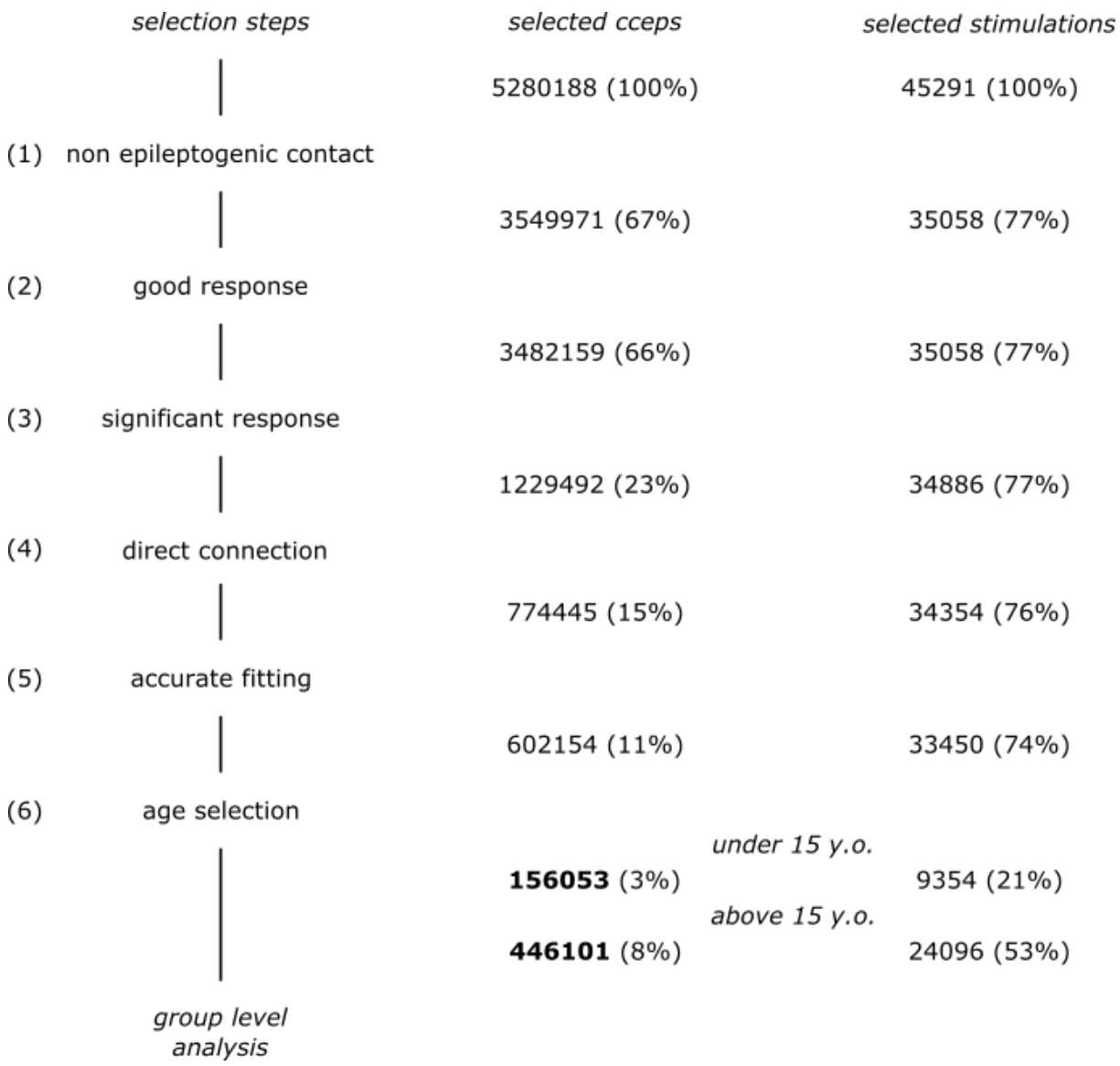

Supplementary Fig. 3 Selection process of CCEPs for the analysis at the group level. A series of steps are successively applied (left column) to select the CCEPs effectively considered in the analysis at the group level. The number of CCEPs available is indicated before and after each selection step (middle column), along with the number of corresponding used stimulations (right column). Percentages of selected CCEPs and stimulations are provided with respect to their initial number (5280188 CCEPs recorded during 45291 stimulations). To be considered in the analysis at the group level, a CCEP needs to be recorded with low enough interictal spike rate (<8.4 spikes/minute) stimulating and recording contact (step 1), a good quality signal (step2), a significant response (step3) within the first 80 ms after the stimulation to decrease the probability of a likely indirect cortico-cortical connections (step4). Following this step, the DCM approach is applied to all selected CCEPs and only accurate estimations are retained (step5). Finally, the CCEP is sorted according to the age of the patient (step 6). Overall, 446101 CCEPs were used at the population level to build the atlas of neuronal delays for the older group (>15 y.o.), and respectively 156053 CCEPs for the younger group (<15 y.o.). Interestingly, the most critical step is the selection of the significant responses (step 3) which removes 65% of the CCEPs selected from the previous step.

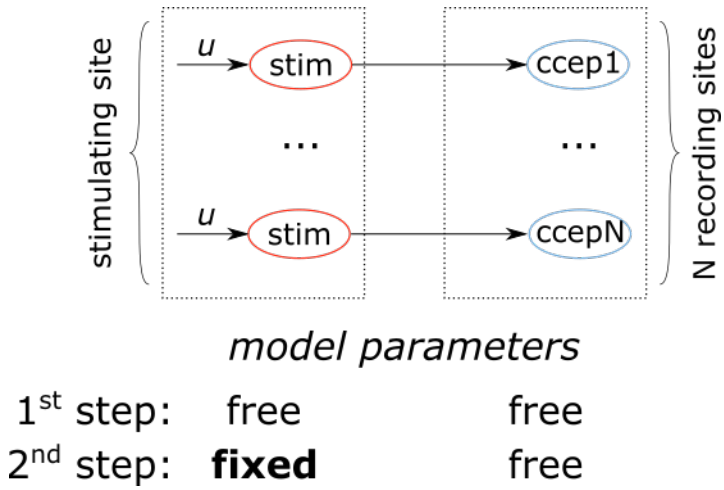

Supplementary Fig. 4 Implementation of the generative Dynamic Causal Model. Due to computational limitations, the global model was splitted into N reduced models, in which the stimulation region was artificially replicated. In a 1st step, transient stimulus input *u* and neuronal parameters were estimated independently for each reduced model. Then, to take into account the uniqueness of the stimulation site, a 2nd step was performed during which the input and the neuronal parameters of the stimulation site were fixed to the averaged estimates of 1st step across the N reduced models; only the neuronal parameters related to the CCEPs were then estimated. This figure is associated to Material and methods (Estimation of axonal conduction delays and synaptic time constants).

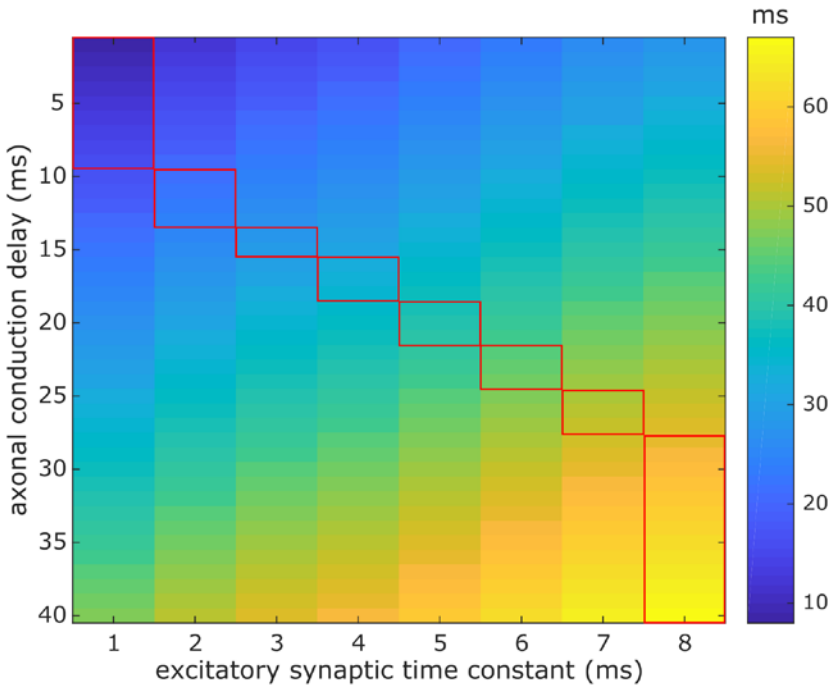

Supplementary Fig. 5 Peak latencies of N1 component predicted by DCM. Vertical axis represents the axonal conduction delays between the stimulating and the recording sites and horizontal axis represents the excitatory synaptic delays of the recording site. For the modelling of each CCEP, one prior for neuronal delays is selected (one red box) so that, at the first iteration of the estimation, the predicted N1 peak latency matches the observed N1 peak latency of the CCEP. This figure is associated to Material and methods (Estimation of axonal conduction delays and synaptic time constants).

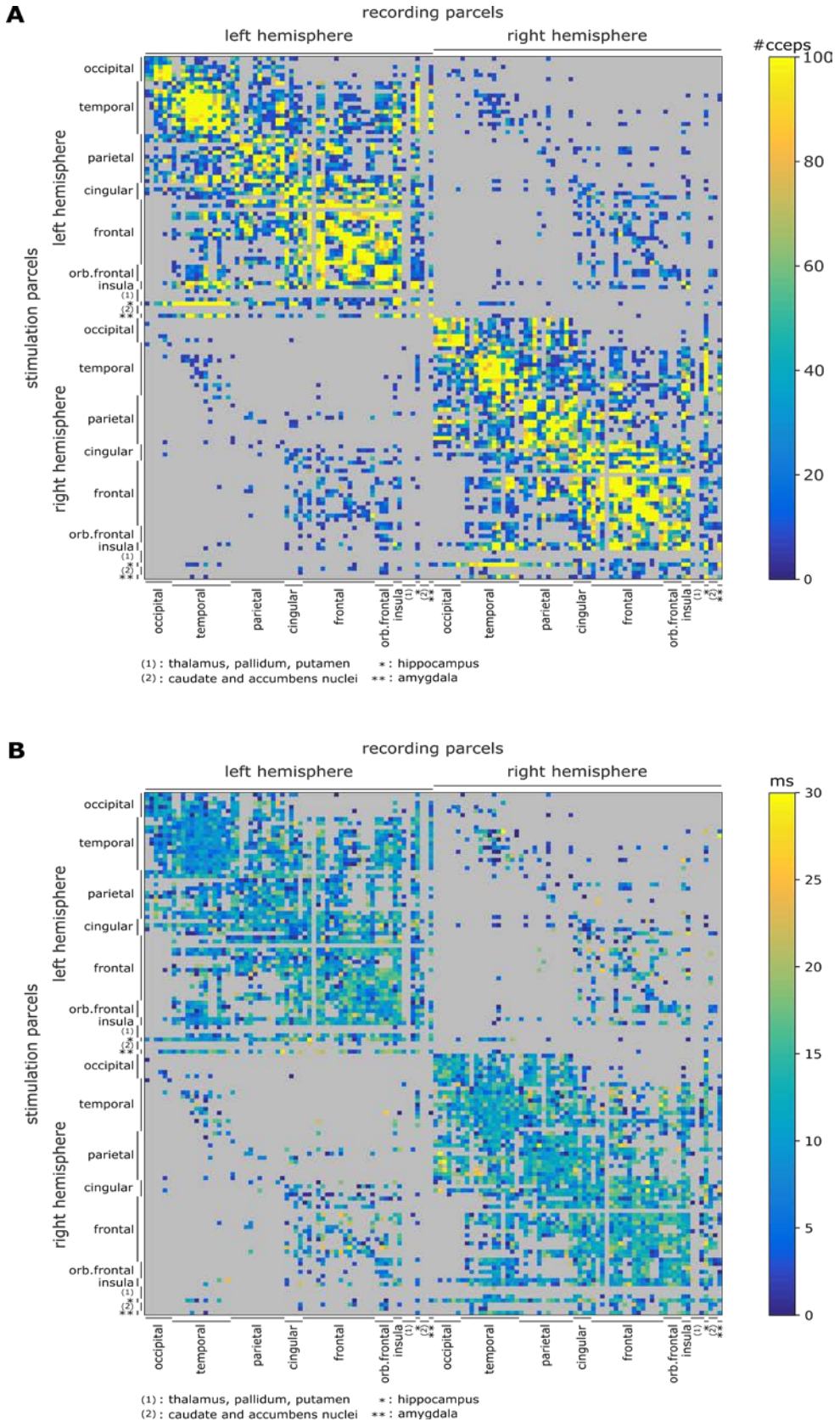

Supplementary Fig. 6 Estimation of axonal conduction delays between brain regions. (A) Numbers of CCEPs and (B) median absolute deviations obtained during the estimation of axonal conduction delays. Results are presented for the older group (>15 y.o.) based on the Lausanne2008-60 parcellation scheme.

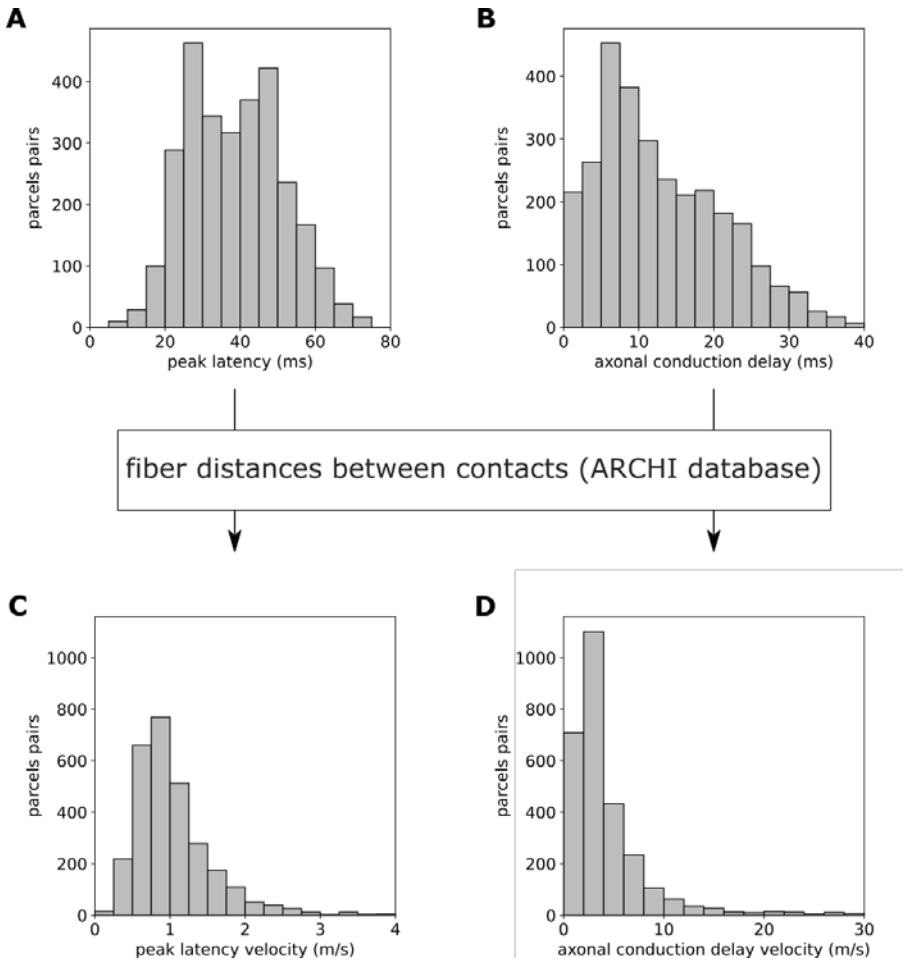

Supplementary Fig. 7 Estimation of conduction velocities. Results are presented for the younger group (<15 y.o.) based on the Lausanne2008-60 parcellation scheme. Distributions of (A) N1 peak latencies (median: 37.5 ms), (B) axonal conduction delays (median: 11.0 ms), and conduction velocities based on (C) N1 peak latencies (median: 0.9 m/s) and (D) axonal conduction delays (median: 3.1 m/s). Distances between stimulating and recording contacts were measured along white matter fibers, using the ARCHI DTI atlas (see section Material and methods (Group level analysis)). This figure is associated to section Results (Mapping of axonal conduction velocities) and Fig. 5.

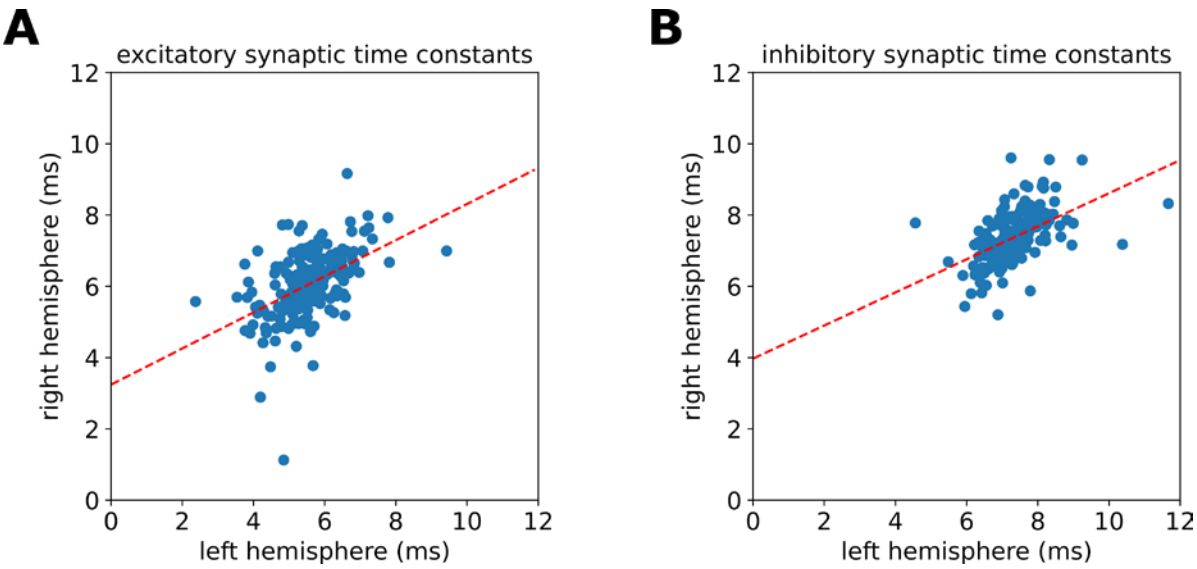

Supplementary Fig. 8 Interhemispheric representation of synaptic time constants. (A) Excitatory and (B) inhibitory synaptic time constants across hemispheres based on the HCP-MMP1 parcellation scheme for the whole group. Each blue dot corresponds to one parcel of the HCP-MMP1 parcellation scheme. Its abscissa (resp. ordinate) is the synaptic time constant of the parcel estimated in the left (resp. right) hemisphere. The red dotted line results from a linear regression between the two hemispheres. Excitatory time constants: slope=0.51, r=0.48, p<1e-10. Inhibitory time constants: slope=0.46, r=0.55, p<1e-14).

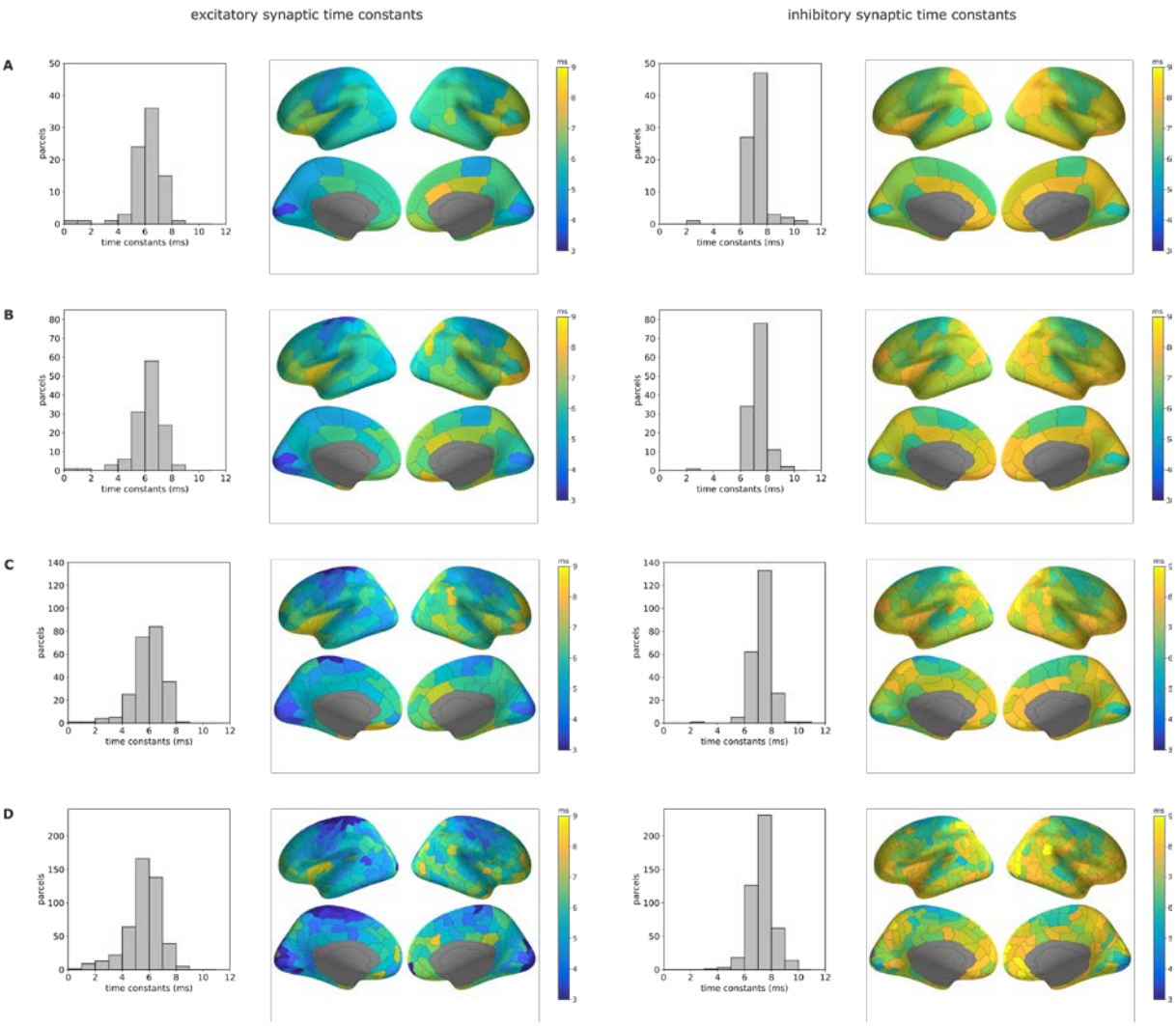

Supplementary Fig. 9 Synaptic time constants. Results are presented for the whole group and for different spatial resolutions of the Lausanne2008 parcellation scheme. At each resolution, the distributions of excitatory and inhibitory synaptic time constants are shown (left), along with the corresponding brain mapping of the excitatory time constants. (A) Lausanne2008-33: 84 parcels (B) Lausanne2008-60: 130 parcels (C) Lausanne2008-125: 235 parcels (D) Lausanne2008-250: 464 parcels. This figure is associated to section Results (Mapping of synaptic time constants) and Fig. 6.

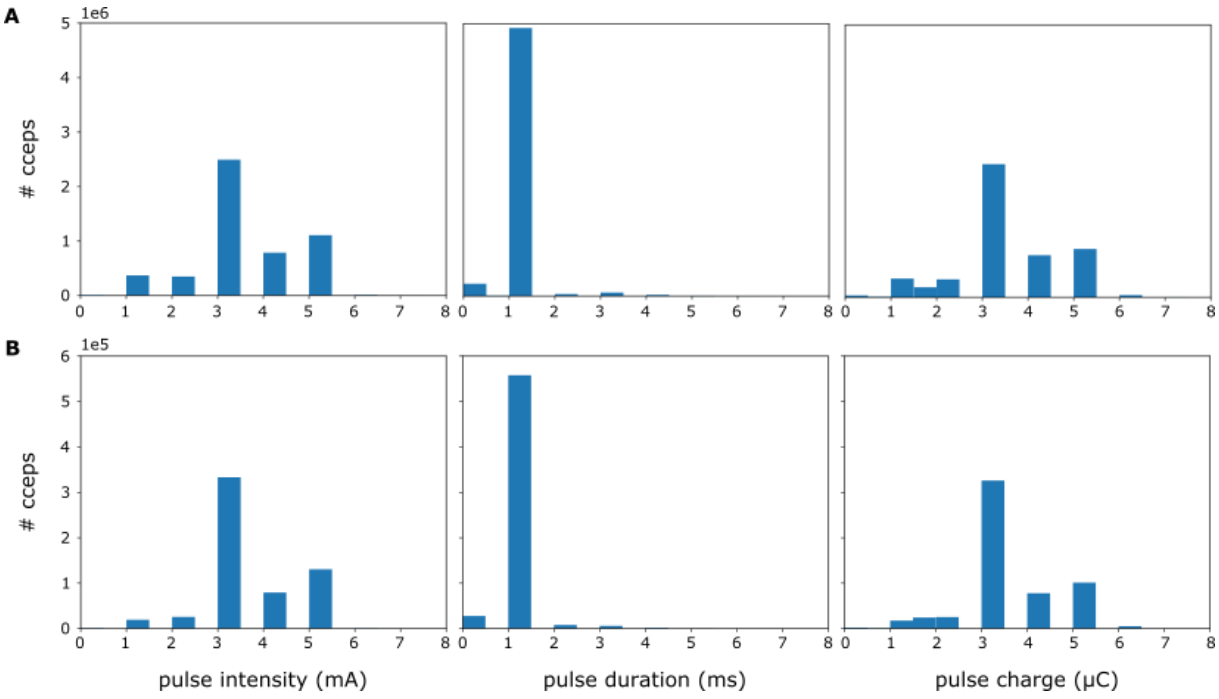

Supplementary Fig. 10 Stimulation parameters. Distribution of stimulation parameters for (A) the complete set of 5280188 CCEPs considered in this study and (B) for the 602154 CCEPs effectively considered for the estimation of the different atlases: pulse intensity (left), duration (middle) and charge (right).

Effect of stimulation parameters

In general, the shape of the CCEP, and thus the derived neural parameters, critically depends on the way electric charges are delivered to the tissue. It can be related directly to the current amplitude and duration[15,38] and to the current waveform[39]. For the results reported in the main text, we did not explicitly model the potential variability of CCEP waveforms due to stimulation parameter changes because we do not estimate there is any significant spatial bias induced by those changes as every epilepsy centers provided data with spatially uniform stimulation. For completeness, we provide in Supplementary Fig. 10 the distributions of stimulation parameters. A precise quantification of CCEP changes as performed in [15] would be of interest but was outside of the scope of this study.

Effect of the contact tissue classification

1) We compared the effect of the tissue classification of the stimulating contacts on the estimation of probability of connection and of axonal conduction delays between regions and confirmed previous results[15] that global probability of connection increased when considering only stimulating contacts located in the white matter; 2) We also observed in this case a global and slight significant increase of peak latencies and axonal conduction delays, along with a decrease of the corresponding velocities (see Supplementary Table 1); 3) Additionally, we compared the effect of the tissue classification of the recording contacts on the estimation of synaptic time constants and noticed a global and small significant decrease of the estimations when only recording contacts located in the white matter were selected. Yet significant, these differences have a reduced impact on the general results (see Supplementary Fig. 11 for the effects on the connectivity of the right insula and on the estimations of synaptic time constants). To further study these differences, for instance those associated to the location of the stimulating contacts, it would be worth highlighting specific connections which could be more affected than others (and represented with a sufficient number of CCEPs), such as the long-range connections between the right insula and the ipsilateral frontal regions, for which the stimulations of contacts located only in the white matter induced shorter axonal conduction delays than stimulations of contacts located only in the gray matter (Supplementary Fig. 11A).

Neuronal characteristic	**Median ± mad**			**p-value**
	all	gray matter	white matter	
Probability of connection	0.54 ± 0.25	0.52 ± 0.28	0.57 ± 0.27	$< 10^{-6}$
Peak latency	35.5 ± 11.2 ms	34.6 ± 11.8 ms	37.0 ± 12.1 ms	$< 10^{-6}$
Axonal conduction delay	9.6 ± 5.5 ms	8.7 ± 5.4 ms	10.6 ± 7.4 ms	$< 10^{-6}$
Peak latency velocity	1.0 ± 0.4 m/s	1.02 ± 0.4 m/s	0.97 ± 0.4 m/s	$< 10^{-6}$
Axonal conduction delay velocity	3.6 ± 2.0 m/s	4.0 ± 2.5 m/s	3.4 ± 2.1 m/s	$< 10^{-6}$
Excitatory synaptic time constant	5.8 ± 0.9 ms	6.1 ± 1.0 ms	5.5 ± 1.1 ms	$< 10^{-6}$
Inhibitory synaptic time constant	7.3 ± 0.7 ms	7.5 ± 0.8 ms	7.1 ± 0.8 ms	$< 10^{-6}$

Supplementary Table 1: Effects of the tissue classification of the CCEPs contacts on the estimations of the neuronal characteristics. Median values and median absolute deviations are given for three groups, based on the tissue classification of the contacts used for the estimation: all (gray or white matter), gray matter only and white matter only. For the first five characteristics, the selection applies to the stimulating contacts and for the last two characteristics, the selection applies to the recording contacts. Values are provided for the parcels, or parcels pairs, estimated conjointly in the 3 groups. Significant differences are assessed between estimations based on contacts located only in the gray matter and contacts located only in the white matter (right column). The first five characteristics were estimated in the older group (>15 y.o.) based on the Lausanne2008-60 parcellation scheme and Wilcoxon signed rank tests were performed between estimations of group 2 and group 3 across parcels pairs (4939 for the probability of connection, 3237 for the others) estimated conjointly in the 3 groups. The last two characteristics were estimated in the whole group based on the HCP-MMP1 parcellation scheme and Wilcoxon signed rank tests were performed between estimations of group 2 and group 3 across the 326 parcels pairs estimated conjointly in the 3 groups.

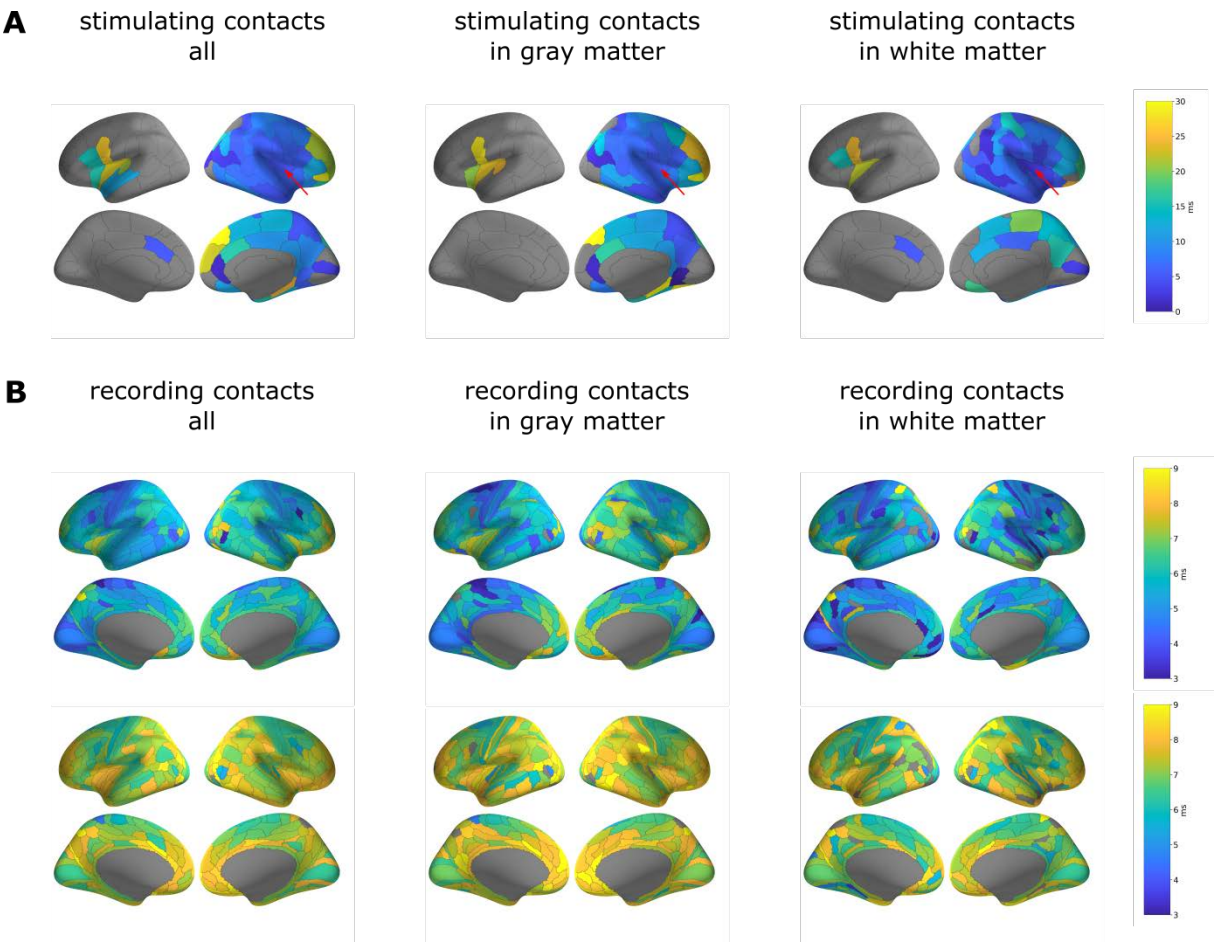

Supplementary Fig. 11 Effect of tissue classification (gray or white matter) of CCEPs contacts on the estimations of neuronal delays. (A) Brain mapping of axonal conduction delays after stimulation of right insula, presented for the older group (>15 y.o.) on the Lausanne2008-60 parcellation scheme and based on the selection of stimulating contacts location: gray or white matter (left), gray matter only (middle) and white matter only (right). The red arrow indicates the right insula. (B) Brain mapping of excitatory (top row) and inhibitory (bottom row) synaptic time constants presented for the whole group on the HCP-MMP1 parcellation scheme and based on the selection of recording contacts location: gray or white matter (left), gray matter only (middle) and white matter only (right).

Effect of the spiking rate threshold

To study the potential impact of this threshold, estimations of neuronal delays based on 3 more restrictive thresholds (respectively 1, 2 and 4 spikes/minute) were performed and compared to the estimations based on the default threshold (Supplementary Fig. 12). Results demonstrated that a higher number of data increases the convergence of the estimations across the different thresholds. This is illustrated with the mapping of neuronal delays computed with a spiking rate threshold of 1 spike/minute (Supplementary Fig. 13). Estimations based on the highest number of CCEPs, as for instance the axonal conduction delays of the insula (Supplementary Fig. 13E) or the synaptic time constants (Supplementary Fig. 13G-H), were the most similar to the ones obtained with the default threshold. Nevertheless, by eliminating so many contacts (Supplementary Fig. 2), such a low threshold has the disadvantage of reducing the possible number of estimations (compare Fig. 3D and Supplementary Fig. 13D to see this effect on the left amygdala). With a higher threshold of 8.4 spikes/minute, the greater presence of potentially pathological CCEPs was counterbalanced and attenuated by a higher number of CCEPs, which enabled to almost provide whole-brain estimates.

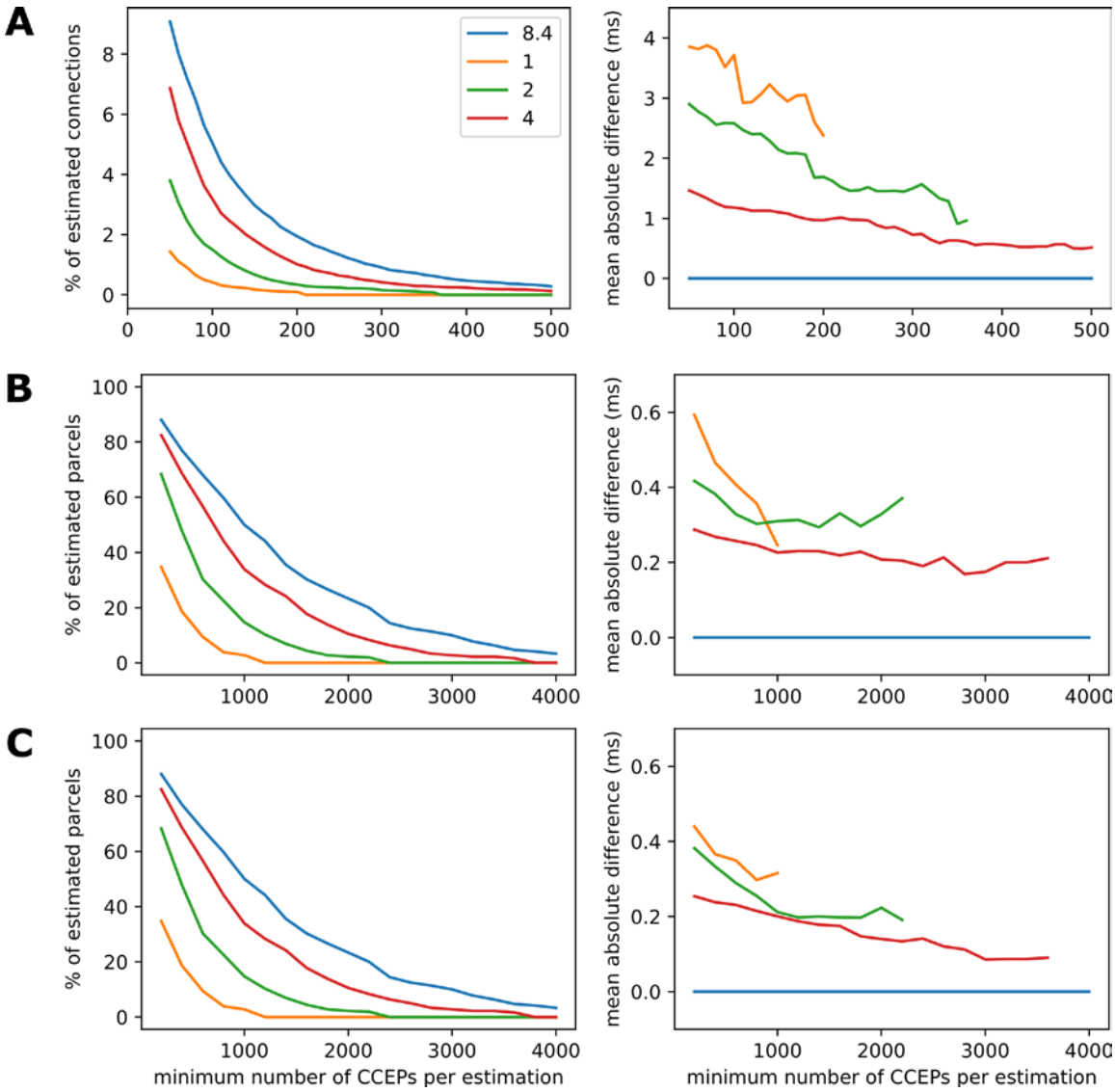

Supplementary Fig. 12 Effect of the spiking rate threshold on the estimations. (A) Axonal conduction delays have been estimated for the 4 thresholds 1, 2, 4 and 8.4 spikes/minute, identified with the same colors across the different panels (see top left panel for the colors). Left panel represents the percentage of estimated connections when varying the minimum number of CCEPs required for the estimation of each connection (same x axis across all panels). Right panel represents the mean absolute difference of the estimations performed with each threshold and the estimations performed with the default threshold used in the study (8.4 spikes/minute). For low thresholds (1 or 2 spikes/minute), the high quantity of rejected CCEPs in addition to a high number of CCEPs required for each estimation cause an absence of estimation. Very interestingly, the results demonstrate that the estimations based on low threshold were closest to the estimations based on the default threshold (8.4 spikes/minute) for those estimations made with the highest number of CCEPs. For instance, between a threshold of 2 spikes/minute (green) and the default threshold (blue), a mean absolute difference of 3 ms (respectively 1 ms) was found for the estimation of axonal conduction delays based on more than 50 CCEPs (respectively 350 CCEPs). (B) Similar to (A) for excitatory synaptic time constants. (C) Similar to (A) for inhibitory synaptic time constants.

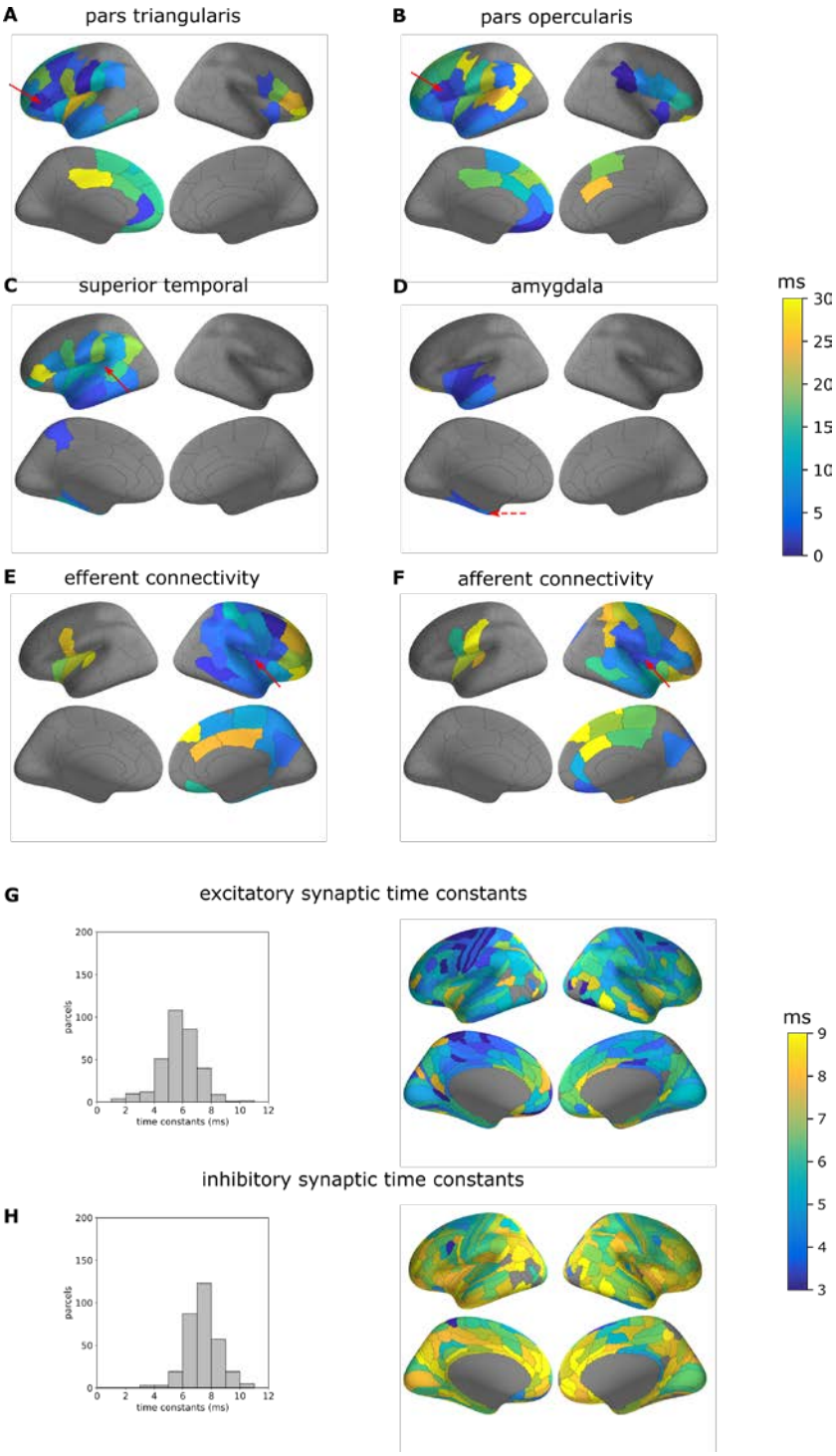

Supplementary Fig. 13 Estimations of neuronal delays with a spiking threshold of 1 spike/minute. (A-D) Mapping of median axonal conduction delays presented for the efferent connections from one stimulated parcel (pointed by a red arrow) to the rest of the brain. Here, the series of stimulated parcels have been chosen in the left hemisphere: (A) the pars triangularis, (B) the pars opercularis, (C) the superior temporal gyrus and (D) the amygdala. (E) Similar to (A) for the right insula. (F) Similar to (A) for the afferent connections of the right insula, which records CCEPs when stimulations are performed in other regions. (A-F) Results are presented for the older group (>15 y.o.) based on the Lausanne2008-60 parcellation scheme. (G) Distribution (left) and brain mapping (right) of excitatory synaptic time constants. Results are presented for the whole group based on the 360 parcels of the HCP-MMP1 parcellation scheme. In grey-colored cortical regions, the estimation was not possible, due to an insufficient amount of data. (H) Similar to (G) for inhibitory synaptic time constants.

References

1. David O, Kiebel SJ, Harrison LM, Mattout J, Kilner JM, Friston KJ. Dynamic causal modeling of evoked responses in EEG and MEG. *NeuroImage*. 2006;30(4):1255-1272. doi:10.1016/j.neuroimage.2005.10.045

2. Ostwald D, Starke L. Probabilistic delay differential equation modeling of event-related potentials. *NeuroImage*. 2016;136:227-257. doi:10.1016/j.neuroimage.2016.04.025

3. Roehri N, Lina J-M, Mosher JC, Bartolomei F, Benar C-G. Time-Frequency Strategies for Increasing High-Frequency Oscillation Detectability in Intracerebral EEG. *IEEE Trans Biomed Eng*. 2016;63(12):2595-2606. doi:10.1109/TBME.2016.2556425